Absorption and production cross sections of K and K^*

A. Martínez Torres[*]
Instituto de Física, Universidade de São Paulo, C.P. 66318, 05389-970 São Paulo, São Paulo, Brazil

K. P. Khemchandani[†]
Universidade Federal de São Paulo, C.P. 01302-907 São Paulo, São Paulo, Brazil

L. M. Abreu[‡]
Instituto de Física, Universidade Federal da Bahia, Campus Universitário de Ondina, 40170-115 Bahia, Brazil

F. S. Navarra[§] and M. Nielsen[‖]
Instituto de Física, Universidade de São Paulo, C.P. 66318, 05389-970 São Paulo, São Paulo, Brazil

(Received 14 September 2017; published 5 March 2018)

We have computed the isospin and spin averaged cross sections of the processes $\pi K^* \to \rho K$ and $\rho K^* \to \pi K$, which are crucial in the determination of the abundances of K^* and K in heavy ion collisions. Improving previous calculations, we have considered several mechanisms which were missing, such as the exchange of axial and vector resonances ($K_1(1270)$, $K_2^*(1430)$, $h_1(1170)$, etc…) and also other processes such as $\pi K^* \to \omega K, \phi K$ and $\omega K^*, \phi K^* \to \pi K$. We find that some of these mechanisms give important contributions to the cross section.

DOI: 10.1103/PhysRevD.97.056001

I. INTRODUCTION

The study of nucleus-nucleus collisions at high energies [1–4], such as Au + Au at center of mass energies of 200 GeV or Pb-Pb at center of mass energies of 2.76 TeV, hints towards the existence of a phase transition from nuclear matter to a locally thermalized state of deconfined quarks and gluons, the quark-gluon plasma (QGP) [5]. After a hot initial stage, the QGP cools and hadronizes forming a hadron gas, where the produced mesons and baryons interact inelastically and the relative abundances are changed. After further cooling, the system reaches chemical equilibrium, where only elastic collisions take place. This is also called "chemical freeze-out" and at this point the abundances are frozen. Finally, at the "kinetic freeze-out," the density becomes small, the interactions no longer occur and the particles stream freely to the detectors [6,7]. After hadronization and before the kinetic freeze-out, the hadrons can interact and different production and absorption reactions (including the formation and decay of resonances) will change the hadron abundances. These changes will be different for different hadron species, and they depend on the details of hadron dynamics, especially on possible resonance formation.

Particularly interesting is the case of the $K^*(892)$ meson. The lifetime of this meson is around 4 fm/c, which is smaller than that of the QGP formed in heavy-ion collisions (∼10 fm/c [7]). This means that, from hadronization up to the kinetic freeze-out, a K^* meson present in the QGP has enough time to decay into K and π. It can also be absorbed, as well as produced, by other mesons present in the medium. All these reactions can change the abundance of the K^* at the kinetic freeze-out.

In Refs. [1–4], K^* production was investigated considering data from Au + Au at center of mass energies of 200 GeV, from Cu + Cu at 62.4 and 200 GeV and from Pb + Pb collisions at 2.76 GeV. Considering the K^* and K transverse momentum spectra and the measured K^*/K yield ratios for all centralities in Au + Au or Cu + Cu compared to the same ratio from $p + p$ collisions, a significant reduction in the K^*/K ratio was found. The measured values were 0.23 ± 0.05 in Au + Au collisions at 200 GeV at RHIC [1] and of 0.19 ± 0.05 in Pb + Pb collisions at 2.76 TeV at LHC [4], while the statistical model predicts

[*]amartine@if.usp.br
[†]kanchan@if.usp.br
[‡]luciano.abreu@ufba.br
[§]navarra@if.usp.br
[‖]mnielsen@if.usp.br

0.33 ± 0.01 in case of Au + Au collisions at 130 GeV at RHIC [8]. In all these collisions, mesons are produced at hadronization, i.e. when quarks and gluons are converted into hadrons, or later, during hadronic scatterings in the hadron gas. Any special feature observed in the measured yields reflects what happens in these two stages.

In Ref. [9], the changes in the K^* and K abundances caused by hadronic scatterings in the hadron gas phase were studied. The authors calculated the cross sections for absorption (and production) of K and K^* by K, K^*, π and ρ. The following processes were considered to account for K absorption: $K\bar{K} \to \pi\pi$, $K\bar{K} \to \rho\rho$ and $K\pi \to K^*$. Similarly the absorption of K^* mesons was attributed to the processes: $K^*\pi \to K\rho$, $K^*\rho \to K\pi$, $K^*\bar{K} \to \rho\pi$, $K^*\bar{K}^* \to \pi\pi$ and $K^*\bar{K}^* \to \rho\rho$. The corresponding production mechanism for K^* and K are simply the inverse reactions of those mentioned above, whose cross sections can be obtained by using the detailed balance principle. These production and absorption cross sections are the most important input entering in the rate equations through which the time evolution of the abundance of both K^* and K, can be obtained. As shown in Ref. [9], due to the interactions of K and K^* with the hadrons present in the medium, the yield associated with the ratio K^*/K decreases by 36% during the expansion of the hadronic matter. The main mechanisms contributing to this reduction were found to be the processes $K^*\pi \to K\rho$, $K^*\rho \to K\pi$, $K^* \to K\pi$ (the corresponding inverse reactions were, of course, also included in the calculation). Considering these processes, an abundance ratio comparable to the RHIC and LHC measurements was found and it was concluded that the measured ratio K^*/K can be explained by the interaction of K^* and K with light mesons in the hadronic medium.

In the determination of the cross sections for the reactions $K^*\pi \to K\rho$ and $K^*\rho \to K\pi$ performed in Ref. [9], some mechanisms were ignored and they could be relevant for the calculation of the K^*/K ratio such as, for instance, the exchange of axial resonances. To consider resonance exchange, though, one needs a reliable information on the mass and width of the resonance as well as the couplings at different resonance-meson-meson vertices. Such information is available in the literature. For example, it was shown in Refs. [10,11] that the $K^*\pi$ interaction and coupled channels (ϕK, ωK, ρK and $K^*\eta$) generate the axial vector meson $K_1(1270)$ state with a two pole structure. The presence of this resonances has been found to be important [11] in describing the invariant mass distribution of the process $K^- p \to K^-\pi^+\pi^- p$ at 63 GeV measured by the WA3 collaboration at CERN [12]. Similarly, the exchange of $K_1(1270)$ could also play an important role when determining the cross section of the reaction $\pi K^* \to \rho K$. Reference [10] also discusses the interaction of $\bar{K}^* K$ and coupled channels in different isospin I and G-parity combinations, which give rise to the following axial resonances listed by the Particle Data Group (PDG) [13]: $h_1(1170)$, $h_1(1380)$ for $I = 0, G = -1$; $f_1(1285)$ for $I = 0, G = +1$; $a_1(1260)$ for $I = 1, G = -1$; $b_1(1235)$ for $I = 1$, $G = +1$. The nature of these resonances has been tested in Refs. [14–16] where their decay widths in several channels were calculated and a good description of the experimental data was found. The inclusion of these resonances can contribute to the cross section of $\rho K^* \to \pi K$.

The main purpose of the present work is to include the exchange of all these resonances in the study of the processes $K^*\pi \to K\rho$ and $K^*\rho \to K\pi$. Besides resonance exchange, some other mechanisms are missing in the determination of the cross sections of $K^*\pi \to K\rho$ and $K^*\rho \to K\pi$ performed in Ref. [9]. For example, the exchange of a vector meson in the t channel and a pseudoscalar in the s channel were taken into account to study the reaction $K^*\pi \to K\rho$, but other mechanisms like u-channel exchange or s-channel exchange of vectors were not. Some of such missing diagrams involve anomalous vertices [17,18] (i.e., the natural parity is not conserved in the vertex, which is described by a Lagrangian containing the Levi-Civita pseudotensor). In Refs. [19,20], it was shown that interaction terms with anomalous parity couplings have a strong impact on the corresponding cross sections, and the relevance of such anomalous terms in the determination of the abundance of $X(3872)$ in heavy ion collisions was computed in Ref. [21]. Such processes, involving the anomalous vertices, were missed in the earlier work of Ref. [22]. Similar is the case of the reaction $K^*\rho \to \pi K$: in Ref. [9] Feynman diagrams related to the exchange of a pseudoscalar meson in the t channel and a vector meson in the s channel were considered. However, other contributions, as u-channel exchange diagrams and exchange of other mesons in the t- and s channels were not taken into account. In this work, we are going to evaluate the contribution from all such mechanisms and calculate the cross sections of the reactions $K^*\pi \to K\rho, K\omega, K\phi$ and $K^*\rho, K^*\omega, K^*\phi \to K\pi$ for the absorption of the K^* meson and the corresponding cross section for its production. We also calculate the corresponding thermal averaged cross sections, which can be useful in the determination of the time evolution of the abundances of K and K^* from heavy ion collisions.

II. FORMALISM

In the model of Ref. [9], the effect of absorption and production of K^* and K mesons in a hadron gas appears in the thermal average cross sections of such processes. These cross sections affect the time evolution of the abundance of K^* and K. As concluded in Ref. [9], the most important absorption and production processes of K^* and K correspond to $\pi K^* \to \rho K$, $\rho K^* \to \pi K$, $K^* \to \pi K$ and the inverse reactions.

In the present work, we calculate these cross sections including the following reactions $\pi K^* \to \rho K, \omega K, \phi K$ and

$\rho K^*, \omega K^*, \phi K^* \to \pi K$. The cross sections associated with the corresponding inverse reactions can be obtained using the principle of detailed balance. Note that in Ref. [9], the cross sections related to processes involving ω and ϕ in the initial or final states were not evaluated in spite of their mass similarity with ρ as well as similar dynamics involved in the corresponding reactions.

We will calculate the cross section of the process $a + b \to c + d$. For a specific reaction mechanism r, we can write σ_r in the center of mass frame as [9,20,22]

$$\sigma_r(s) = \frac{1}{16\pi\lambda(s, m_{a,r}^2, m_{b,r}^2)} \int_{t_{\min,r}}^{t_{\max,r}} dt \bar{\sum_{S,I}} |\mathcal{M}_r(s,t)|^2, \quad (1)$$

where s and t are the Mandelstam variables for the reaction r, $m_{a,r}$ and $m_{b,r}$ represent the masses of the two particles in the initial state of the reaction r, $\lambda(a,b,c)$ is the Källén function and $\mathcal{M}_r$ is the reduced matrix element for the process r.

The symbol $\bar{\sum}_{S,I}$ in Eq. (1) represents the sum over the spins (S) and isospins (I) projections of the particles in the initial and final states, weighted by the isospin and spin degeneracy factors of the two particles forming the initial state for the reaction r, i.e.,

$$\bar{\sum_{S,I}} |\mathcal{M}_r|^2 \to \frac{1}{(2I_{a,r}+1)(2I_{b,r}+1)} \frac{1}{(2s_{a,r}+1)(2s_{b,r}+1)} \times \sum_{S,I} |\mathcal{M}_r|^2, \quad (2)$$

where,

$$\sum_{S,I} |\mathcal{M}_r|^2 = \sum_{i,j} \left[\sum_{S} |\mathcal{M}^{ij}|^2 \right]. \quad (3)$$

In Eq. (3), i and j represent the initial $(a+b)$ and final $(c+d)$ channels in the reaction r for a particular charge $Q_r = Q_a + Q_b = Q_c + Q_d = -1, 0, +1, +2$.

In Figs. 1 and 2, we show the different diagrams contributing to the processes $\pi K^* \to \rho K, \omega K, \phi K$ and $\rho K^*, \omega K^*, \phi K^* \to \pi K$ (without specifying the charge of the reaction).

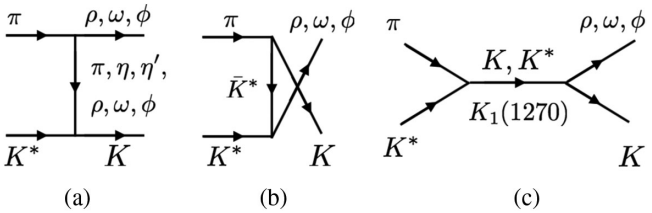

FIG. 1. Diagrams contributing to the processes $\pi K^* \to \rho K$, $\omega K, \phi K$ in the t channel (a), u channel (b) and s channel (c).

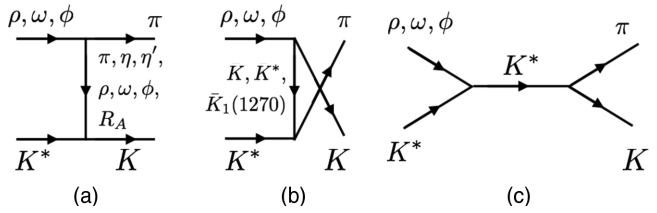

FIG. 2. Diagrams contributing to the processes $\rho K^*, \omega K^*$, $\phi K^* \to \pi K$ in the t channel (a), u channel (b) and s channel (c). The symbol R_A represents the exchange of the axial resonances $h_1(1170)$, $h_1(1380)$, $f_1(1285)$, $a_1(1260)$ and $b_1(1235)$ listed by the PDG and found from the dynamics in the $\bar{K}^* K$ system and coupled channels [10].

Each of the amplitudes $\mathcal{M}^{ij}$ of Eq. (3) can be written as

$$\mathcal{M}^{ij} = T^{ij} + U^{ij} + S^{ij}, \quad (4)$$

where T^{ij}, U^{ij} and S^{ij} are the contributions related to the t-, u- and s-channel diagrams shown in Figs. 1 and 2 for the process $i \to j$ for a particular total charge of the reaction r.

The amplitudes for these t-, u- and s- channel diagrams are determined by considering Lagrangians for the Pseudoscalar-Pseudoscalar-Vector (PPV), Vector-Vector-Pseudoscalar (VVP) and Vector-Vector-Vector (VVV) vertices. These Lagrangians are based on an effective theory in which the vector mesons are identified as the dynamical gauge bosons of the hidden $U(3)_V$ local symmetry in the $U(3)_L \times U(3)_R/U(3)_V$ nonlinear sigma model [23–26], obtaining

$$\begin{aligned} \mathcal{L}_{PPV} &= -ig_{PPV}\langle V^\mu [P, \partial_\mu P]\rangle, \\ \mathcal{L}_{VVP} &= \frac{g_{VVP}}{\sqrt{2}} \epsilon^{\mu\nu\alpha\beta} \langle \partial_\mu V_\nu \partial_\alpha V_\beta P\rangle \\ \mathcal{L}_{VVV} &= ig_{VVV}\langle (V^\mu \partial_\nu V_\mu - \partial_\nu V_\mu V^\mu) V^\nu)\rangle. \end{aligned} \quad (5)$$

The $\mathcal{L}_{VVP}$ Lagrangian written above contains the Levi-Civita pseudotensor since it describes an anomalous vertex, which involves a violation of the natural parity in the vertex [17,18]. In Eq. (5), P and V_μ are matrices containing the octet of pseudoscalars and vectors mesons and the singlet of SU(3), respectively, which in the physical basis and considering ideal mixing for η and η' as well as for ω and ϕ read as [10,11,27]:

$$P = \begin{pmatrix} \frac{\eta}{\sqrt{3}} + \frac{\eta'}{\sqrt{6}} + \frac{\pi^0}{\sqrt{2}} & \pi^+ & K^+ \\ \pi^- & \frac{\eta}{\sqrt{3}} + \frac{\eta'}{\sqrt{6}} - \frac{\pi^0}{\sqrt{2}} & K^0 \\ K^- & \bar{K}^0 & -\frac{\eta}{\sqrt{3}} + \sqrt{\frac{2}{3}}\eta' \end{pmatrix}, \quad (6)$$

$$V_\mu = \begin{pmatrix} \frac{\omega+\rho^0}{\sqrt{2}} & \rho^+ & K^{*+} \\ \rho^- & \frac{\omega-\rho^0}{\sqrt{2}} & K^{*0} \\ K^{*-} & \bar{K}^{*0} & \phi \end{pmatrix}_\mu . \tag{7}$$

The couplings appearing in Eq. (5) are given by [28–30]

$$g_{PPV} = \frac{m_V}{2f_\pi}, \qquad g_{VVP} = \frac{3m_V^2}{16\pi^2 f_\pi^3}, \qquad g_{VVV} = \frac{m_V}{2f_\pi}, \tag{8}$$

with m_V being the mass of the vector meson, which we take as the mass of the ρ meson, and $f_\pi = 93$ MeV is the pion decay constant. These couplings can be considered as phenomenological couplings, in the sense that they can be directly used to reproduce relevant experimental data related to branching ratios, partial decay widths of vector mesons, etc. The symbol $\langle\rangle$ in Eq. (5) indicates the trace in the isospin space.

The evaluation of some of the diagrams in Figs. 1 and 2 requires the coupling of several axial resonances to their hadron components. This couplings are directly taken from Refs. [10,11], and we list them in Tables I and II of Appendix A for the convenience of the reader.

After defining all the ingredients needed for the evaluation of the contribution of the diagrams in Figs. 1 and 2, we can start writing the contributions explicitly. The t-channel, T^{ij}, u-channel, U^{ij}, and s-channel, S^{ij}, amplitudes for the diagrams shown in Figs. 1(a), 1(b), and 1(c), respectively, for a reaction r of the type $i(a+b) \to j(c+d)$ are given by

$$T^{ij} = \sum_k \mathbb{T}_k^{ij} g_{PPV}^2 \epsilon^\mu(k)\epsilon^\nu(p') k'_\mu p_\nu \frac{1}{t - m_{P_k}^2 + i\epsilon} + \sum_k \bar{\mathbb{T}}_k^{ij} g_{VVP}^2 \epsilon^{\mu\nu\alpha\beta}\epsilon^{\mu'\nu'\alpha'}{}_\beta p'_\mu p_\alpha k_{\mu'} k'_{\alpha'} \epsilon_\nu(p')\epsilon_{\nu'}(k) \frac{1}{t - m_{V_k}^2 + i\Gamma_{V_k} m_{V_k}}, \tag{9}$$

$$U^{ij} = \sum_k \mathbb{U}_k^{ij} g_{VVV} g_{PPV} \frac{1}{u - m_{V_k}^2 + i\Gamma_{V_k} m_{V_k}} \epsilon^\mu(k)\epsilon^\nu(p') \times \left[2\left(-1 + \frac{m_\pi^2 - m_K^2}{m_{V_k}^2}\right)(k_\nu p_\mu + p'_\mu p_\nu) - 2\left(1 + \frac{m_\pi^2 - m_K^2}{m_{V_k}^2}\right)(k_\nu k'_\mu + p'_\mu k'_\nu) - g_{\nu\mu}\left\{ -2(k'+p)\cdot p' + (m_\pi^2 - m_K^2)\left(1 + \frac{m_\rho^2 - m_{K^*}^2}{m_{V_k}^2}\right)\right\}\right], \tag{10}$$

$$S^{ij} = \mathbb{S}_K^{ij} g_{PPV}^2 \epsilon^\mu(k)\epsilon^\nu(p') p_\mu k'_\nu \frac{1}{s - m_K^2 + i\epsilon} + \mathbb{S}_{K^*}^{ij} g_{VVP}^2 \epsilon^{\mu\nu\alpha\beta}\epsilon^{\mu'\nu'\alpha'}{}_\beta \epsilon_\nu(k)\epsilon_{\nu'}(p') k_\mu p'_{\mu'} p_\alpha k'_{\alpha'} \frac{1}{s - m_{K^*}^2 + i\Gamma_{K^*} m_{K^*}} + \sum_{l=1}^{2} \frac{g_{K_1,l}^{(i)} g_{K_1,l}^{(j)}}{s - M_{K_1,l}^2 + i\Gamma_{K_1,l} M_{K_1,l}} \left[-g_{\mu\nu} + \frac{p_\mu k'_\nu}{M_{K_1,l}^2}\right] \epsilon^\mu(k)\epsilon^\nu(p'), \tag{11}$$

where $\mathbb{T}_k^{ij}$, $\bar{\mathbb{T}}_k^{ij}$, $\mathbb{U}_k^{ij}$, $\mathbb{S}_K^{ij}$ and $\mathbb{S}_{K^*}^{ij}$ are coefficients which depend on the initial i and final j channels, as well as the exchanged particle k, and they are given in Tables III–VII of Appendix A. In Eqs. (9), (10) and (11), p, k are, respectively, the four-momentum of the π and K^* in the initial state, and p' and k' correspond, respectively, to the four-momentum of the vector meson (ρ, ω or ϕ) and the K in the final state, $\epsilon^{\mu\nu\alpha\beta}$ is the Levi-Civita tensor and $\epsilon_\mu(q)$ is the polarization vector associated with the particle exchanged, with four momentum q. To arrive to these expressions we have made use of the Lorenz gauge, in which $\epsilon(p)\cdot p = 0$, and the fact that the contraction of an antisymmetric tensor, like the Levi-Civita tensor, with a symmetric one gives 0. The m_{P_k} in Eq. (9) corresponds to the mass of the exchanged pseudoscalar in Fig. 1(a) and m_{V_k} and Γ_{V_k} are the mass and width, respectively, of the exchanged vector. We have considered [13] $\Gamma_\phi = 4.3$, $\Gamma_\omega = 8.5$, $\Gamma_{K^*} = 50.5$ and $\Gamma_\rho = 149.4$ MeV and used isospin average masses, $m_\rho = 770$, $m_\omega = 782$, $m_{K^*} = 892$, $m_\phi = 1020$, $m_\pi = 137$ and $m_K = 496$ MeV. The consideration of the widths in the propagators of the unstable mesons [in Eqs. (10) and (11)] can be interpreted as taking self-energy corrections into account by considering a Breit-Wigner distribution for the unstable particles. Such corrections can be regarded as compatible with the phenomenological couplings in Eq. (8).

In Eqs. (10) and (11), $g_{\alpha\beta}$ is the Minkowski metric tensor. The $M_{K_1,l}$, $\Gamma_{K_1,l}$ and $g^{(i)}_{K_1,l}$ and $g^{(j)}_{K_1,l}$ present in Eq. (11) are the mass, width and coupling of the pole l (to the initial i and final j channels) associated with the axial state $K_1(1270)$. These values can be found in Table I of Appendix A. In the case of the t-channel amplitude of Eq. (9), we have considered the exchange of pseudoscalars as well as vector mesons. A note here is in order. When exchanging a pion in the t channel in the reaction $\pi K^* \to \rho K$, the energy-momentum conservation in the vertex $\pi \to \pi\rho$ of Fig. 1(a) is such that the exchanged pion can become on-shell. Because of this, in some regions of the phase-space, the pion propagator develops a pole originating a singular cross section [31,32]. This latter singularity in the cross section can be removed by the so-called Peierls method [31], where the basic idea is to introduce a complex four-momentum for the unstable particle in the vertex by considering its decay width. As a consequence, the four-momentum of the exchanged particle gets an imaginary part through the energy-momentum conservation, which leads to [31,32]

$$\frac{1}{t-m_\pi^2+i\epsilon} \to \frac{1}{t-m_\pi^2-im_\rho\Gamma_\rho\frac{E_\rho-E_\pi}{E_\rho}}, \tag{12}$$

where E_π and E_ρ are the energies for the external ρ and π in the center of mass frame. Note that the origin of the imaginary part in Eq. (12) lies in the definition of the Mandelstam variable t when the unstable nature of the particle in the vertex is incorporated. For instance, at the $\rho\pi\pi$ vertex in Fig. 1(a), the Mandelstam t variable is defined as $t=(p-p')^2$. If we consider ρ as a stable particle, then

$$t=(p-p')^2=m_\pi^2+m_\rho^2-2E_\rho E_\pi+2\vec{p}_\rho\cdot\vec{p}_\pi=m_\pi^2+m_\rho^2-2\sqrt{m_\rho^2+\vec{p}_\rho^{\,2}}E_\pi+2\vec{p}_\rho\cdot\vec{p}_\pi \tag{13}$$

Substituting $m_\rho^2 \to m_\rho^2 - im_\rho\Gamma_\rho$, we can write

$$\begin{aligned}(p-p')^2 &= m_\pi^2+m_\rho^2-im_\rho\Gamma_\rho-2\sqrt{m_\rho^2-im_\rho\Gamma_\rho+\vec{p}_\rho^{\,2}}E_\pi+2\vec{p}_\rho\cdot\vec{p}_\pi\\ &= m_\pi^2+m_\rho^2-im_\rho\Gamma_\rho-2\sqrt{E_\rho^2-im_\rho\Gamma_\rho}E_\pi+2\vec{p}_\rho\cdot\vec{p}_\pi\\ &\simeq m_\pi^2+m_\rho^2-im_\rho\Gamma_\rho-2E_\rho\left(1-i\frac{m_\rho\Gamma_\rho}{2E_\rho^2}\right)E_\pi+2\vec{p}_\rho\cdot\vec{p}_\pi\\ &= t-im_\rho\Gamma_\rho\left(1-\frac{E_\pi}{E_\rho}\right),\end{aligned} \tag{14}$$

where t is the definition of the Mandelstam variable calculated by treating ρ as a stable particle [Eq. (13)].

For the u-channel amplitude we can only have exchange of vector mesons, since the exchange of a pseudoscalar meson implies a vertex which would violate either parity or angular momentum. For the case of the s-channel amplitude, we have considered exchange of pseudoscalars, vector mesons and resonances, with the only possibilities compatible with conservation of quantum numbers being the pseudoscalar K, the vector K^* and the state $K_1(1270)$.

In the case of the t-, u- and s-channel diagrams in Figs. 2(a)–2(c), respectively, we find the following contributions,

$$\begin{aligned}\boldsymbol{T}^{ij} &= \sum_k \mathcal{T}^{ij}_k g^2_{PPV}\epsilon^\mu(p)\epsilon^\nu(k)p'_\mu k'_\nu\frac{1}{t-m^2_{P_k}+i\epsilon}\\ &+\sum_k \bar{\mathcal{T}}^{ij}_k g^2_{VVP}\epsilon^{\mu\nu\alpha\beta}\epsilon^{\mu'\nu'\alpha'}{}_\beta\epsilon_\nu(p)\epsilon_{\nu'}(k)p_\mu p'_\alpha k_{\mu'}k'_{\alpha'}\frac{1}{t-m^2_{V_k}+i\Gamma_{V_k}m_{V_k}}\\ &-\sum_A\frac{g_A^{(1)}g_A^{(2)}}{t-M_A^2+i\Gamma_A M_A}\left[g_{\mu\nu}+\frac{p'_\mu k'_\nu}{M_A^2}\right]\epsilon^\mu(p)\epsilon^\nu(k),\end{aligned} \tag{15}$$

$$\begin{aligned}\boldsymbol{U}^{ij} &= \mathcal{U}^{ij}_{\bar{K}} g^2_{PPV}\epsilon^\mu(p)\epsilon^\nu(k)k'_\mu p'_\nu\frac{1}{u-m^2_{\bar{K}}+i\epsilon}\\ &+\mathcal{U}^{ij}_{\bar{K}^*} g^2_{VVP}\epsilon^{\mu\nu\alpha\beta}\epsilon^{\mu'\nu'\alpha'}{}_\beta\epsilon_\nu(p)\epsilon_{\nu'}(k)p_\mu k'_\alpha k_{\mu'}p'_{\alpha'}\frac{1}{u-m^2_{\bar{K}^*}+i\Gamma_{\bar{K}^*}m_{\bar{K}^*}}\\ &-\sum_{l=1}^{2}\frac{g^{(1)}_{K_1,l}g^{(2)}_{K_1,l}}{u-M^2_{K_1,l}+i\Gamma_{K_1,l}M_{K_1,l}}\left[g_{\mu\nu}+\frac{k'_\mu p'_\nu}{M^2_{K_1,l}}\right]\epsilon^\mu(p)\epsilon^\nu(k),\end{aligned} \tag{16}$$

$$S^{ij} = \sum_k \mathcal{S}^{ij} g_{PPV} g_{VVV} \left[\left\{ (m_{K^*}^2 - m_V^2) \left(1 - \frac{m_K^2 - m_\pi^2}{m_{V_k}^2} \right) - 2(k \cdot p' - p \cdot p') \right\} \epsilon(k) \cdot \epsilon(p) \right.$$
$$\left. - 2(k_\mu k'_\nu + p'_\mu p_\nu - k_\mu p'_\nu - k'_\mu p_\nu) \epsilon^\mu(p) \epsilon^\nu(k) \right] \frac{1}{s - m_{V_k}^2 + i\Gamma_{V_k} m_{V_k}}, \tag{17}$$

where $\mathcal{T}^{ij}$, $\bar{\mathcal{T}}^{ij}$, $\mathcal{U}^{ij}_{\bar{K}}$, $\mathcal{U}^{ij}_{\bar{K}^*}$ and $\mathcal{S}^{ij}$ are coefficients which are given in Tables VIII–XII of Appendix A. In Eqs. (15), (16), (17), and all diagrams depicted in Fig. 2, p, k are, respectively, the four momenta of the external vector meson without strangeness (ρ, ω, or ϕ) and of the external K^*, while p' and k' are the four momenta of the external π and K, respectively. The symbols M_A, Γ_A, $g_A^{(1)}$ and $g_A^{(2)}$ in Eq. (15) represent, respectively, the mass, width and coupling constants to the two vertices shown in Fig. 2(a) for the pole associated with the exchanged axial resonance R_A (see Table II of Appendix A for the numerical values). In Eq. (16), $M_{K_1,l}$, $\Gamma_{K_1,l}$, $g^{(1)}_{K_1,l}$ and $g^{(2)}_{K_1,l}$ correspond to the mass, width and coupling constants to the two vertices shown in Fig. 2(b) for the pole l related to the $K_1(1270)$ state and their numerical values are listed in Table I of Appendix A. In Eq. (17), m_V is the mass of the external ρ, ω or ϕ vector mesons and, as in case of Eq. (10), m_{V_k} and Γ_{V_k} are the mass and width, respectively, of the exchanged vector meson in the diagram of Fig. 2(b). Note that, in this case, we cannot have the exchange of a pseudoscalar meson in the s channel, since it implies the presence of a three pseudoscalar vertex.

Before proceeding with the discussion on the results found in our work, some comments are here in order related to the present approach:

(i) The couplings of the exchanged resonances to the different meson-meson channels, listed in Tables I, II, XIII are complex in nature, which may raise a question related to the unitarity of such amplitudes. As shown in Refs. [10,11], these couplings are obtained from the scattering matrix found by solving the Bether-Salpeter equation in the complex energy plane. In the vicinity of the resonance, the scattering matrix (found from the resolution of the Bethe-Salpeter equation in coupled channels) for a process $a + b \to c + d$ can be written in terms of a Breit-Wigner propagator for the generated resonance in the system times the couplings of this resonance to the channels $a + b$ and $c + d$. Thus, the complex amplitudes obtained by using the couplings in Tables I, II, XIII correspond to the complex amplitudes which result from solving the Bethe-Salpeter equation, and which are manifestly unitary.

(ii) In the present work, two different sources of interactions are considered, one which corresponds to the dynamical generation of the resonances in the system (incorporated by means of the couplings given in Refs. [10,11]). And the other arising from those diagrams which are not required to generate the resonances found in Refs. [10,11]. The former one is equivalent to unitarizing the interactions considered in Refs. [10,11] while the latter interactions are not unitarized, since it is not expected that the unitarization of diagrams different to those considered in Refs. [10,11] should affect much the generation of the resonances found in those works. Ideally, one should unitarize the interactions coming from all sources, but as a first attempt to show the possible importance of the missing diagrams and processes in Ref. [9], we have adopted a simplified, but practical, approach. More complete calculations are beyond the scope of the present work.

III. RESULTS

A. Cross sections for the processes $\pi K^* \to \rho K, \omega K, \phi K$

We start the discussion of the results by showing, in Fig. 3, the cross sections obtained from Eq. (1) for the reaction $\pi K^* \to \rho K$ with different mechanisms: (1) t-channel exchange of a pseudoscalar meson (solid line with circles); (2) t-channel exchange of a vector meson

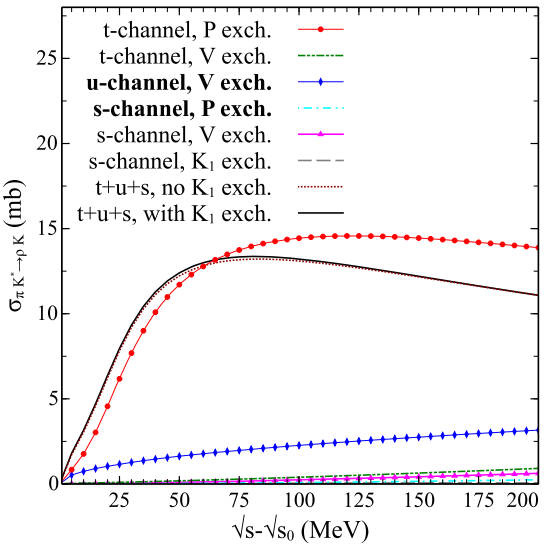

FIG. 3. Cross sections obtained with Eq. (1) for the process $\pi K^* \to \rho K$ considering different mechanism as a function of $\sqrt{s} - \sqrt{s_0}$, where $\sqrt{s}$ is the center of mass energy and $\sqrt{s_0}$ is the threshold energy for the reaction. The boldfaced text in the legends indicate the mechanisms considered in Ref. [9].

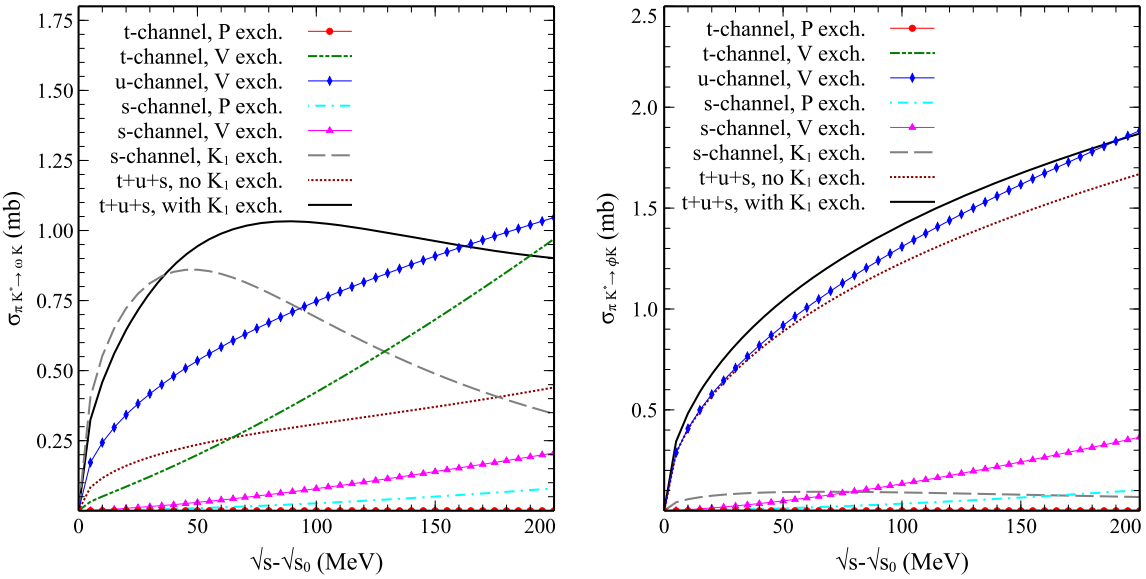

FIG. 4. Cross sections obtained with Eq. (1) for the process $\pi K^* \to \omega K$ (left panel) and $\pi K^* \to \phi K$ (right panel) considering different mechanism as a function of $\sqrt{s} - \sqrt{s_0}$, where $\sqrt{s}$ is the center of mass energy and $\sqrt{s_0}$ is the threshold energy for the reaction. None of these processes were evaluated in Ref. [9].

(dashed-dotted-dotted line); (3) u-channel exchange of a vector (line with rhombus); (4) s-channel exchange of a pseudoscalar (dashed-dotted line); (5) s-channel exchange of a vector (solid line with triangles) (6) s-channel exchange of $K_1(1270)$ (dashed line). The dotted and solid lines in Fig. 3 correspond, respectively, to considering the mechanisms (1)–(5) and (1)–(6) for the determination of the cross section.

As can be seen in Fig. 3, the contribution from the t-channel exchange of a pseudoscalar meson (not considered in Ref. [9]) gives rise to the largest cross section and the other mechanisms considered produce small corrections to it. Note that due to a reordering of the particles in the vertices, the t-channel (u-channel) exchange in Ref. [9] corresponds to the u-channel (t-channel) exchange in the present work to which we refer throughout the text. It is also interesting to notice that the u-channel exchange of a vector meson (considered in Ref. [9]) leads to a larger cross section than that associated with the t-channel exchange of a vector meson (not evaluated in Ref. [9]) and the s-channel exchange of a pseudoscalar. The process in which a vector meson is exchanged in the s channel (not taken into account in Ref. [9]) gives a larger contribution to the cross section when compared with the one arising from the exchange of a pseudoscalar in the s channel (considered in Ref. [9]). It should be mentioned that the contribution of the $K_1(1270)$ exchange in the s channel to the cross section is negligible (compare the solid and dotted lines of Fig. 3).

In Fig. 4, we show the results for the reactions $\pi K^* \to \omega K$ (left panel) and $\pi K^* \to \phi K$ (right panel), reactions which were not considered in Ref. [9]. As can be seen, the final cross section for both reactions (solid lines) have similar magnitude and both are smaller than the one for the process $\pi K^* \to \rho K$ (solid line in Fig. 3) by around one order of magnitude. This finding indicates that the absorption mechanism of a K^* by a pion, producing a K together with an ω or a ϕ may probably not be relevant in the determination of the time evolution of the abundances found in Ref. [9] for K^* and K. Note, however, that without the contribution to the cross section of $\pi K^* \to \rho K$ from a diagram involving $\rho\pi\pi$ and $K^*\pi K$ vertices (not evaluated in Ref. [9]), shown as line with circles in Fig. 3, the cross sections for the processes $\pi K^* \to \rho K, \omega K, \phi K$ are comparable. It is also interesting to notice the relevance in the $\pi K^* \to \omega K$ cross section of the mechanism in which the $K_1(1270)$ is exchanged in the s channel (dashed line in Fig. 4, left panel). The inclusion of such $K_1(1270)$ exchange produces a significant change in the cross section, as can be noticed from Fig. 4 by comparing the dotted line, which shows the total cross section obtained without considering the exchange of $K_1(1270)$ in the s channel, and the solid line, which corresponds to the result with such an exchange included. As in case of the process $\pi K^* \to \rho K$, the u-channel exchange of a vector meson in the reactions $\pi K^* \to \omega K$ and $\pi K^* \to \phi K$ (line with rhombus in both panels of Fig. 4) gives larger contribution to the cross section than the exchange of a vector or pseudoscalar mesons in the s channel or a vector meson in the t channel, with the latter mechanism being more important in case of the process $\pi K^* \to \omega K$.

B. Cross sections for the processes $\rho K^*, \omega K^*, \phi K^* \to \pi K$

In Fig. 5, we show the cross section calculated with Eq. (1) for the process $\rho K^* \to \pi K$ considering

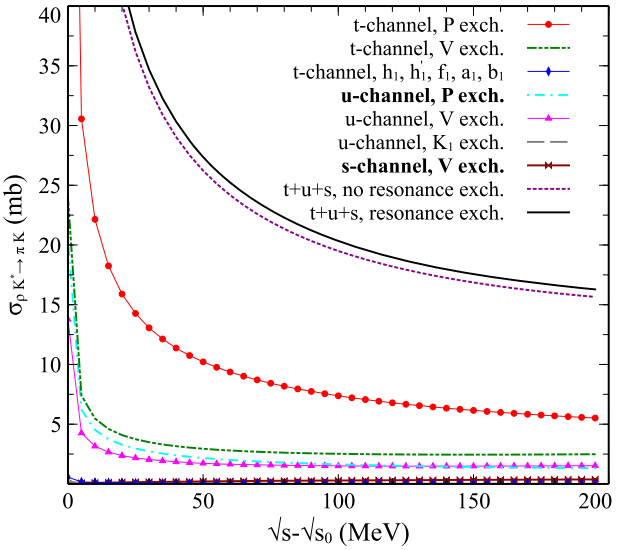

FIG. 5. Cross sections obtained with Eq. (1) for the process $\rho K^* \to \pi K$ considering different mechanism as a function of $\sqrt{s} - \sqrt{s_0}$, where $\sqrt{s}$ is the center of mass energy and $\sqrt{s_0}$ is the threshold energy for the reaction. Since the cross section, independently of the mechanism, diverges at the threshold, they have been calculated at an energy starting 0.5 MeV above the threshold of the reaction, so the x axis is actually $\sqrt{s} - \sqrt{s_0} + 0.5$ MeV. In the figure, $h_1 \equiv h_1(1170)$ and $h_1' \equiv h_1(1380)$. The boldfaced text in the legends indicates the mechanism evaluated in Ref. [9].

contributions from the mechanism shown in Figs. 2(a)–2(c). Since the process is exothermic, the cross section diverges at the threshold. As can be seen, the consideration of the exchange of the resonances listed in Table II in the t channel and the exchange of $K_1(1270)$ in the u channel produces a small modification in the total cross section. The contribution to the cross section from the exchange of a pseudoscalar meson in the t channel is larger than that related to the exchange of a vector meson in the t or u channel (both missing in Ref. [9]) and that of a pseudoscalar meson in the u channel (considered in Ref. [9]). Since the s-channel exchange of a vector meson (taken into account in Ref. [9]) turns out to give a very small contribution to the cross section, the other mechanisms considered here become relevant.

Similar to the case $\rho K^* \to \pi K$, the resonance exchange in the t and u channels for the reactions $\omega K^* \to \pi K$ and $\phi K^* \to \pi K$ produces a weak modification in the cross section (compare the solid and dotted lines in both panels of Fig. 6). Interestingly, the final cross sections for $\rho K^* \to \pi K$, $\omega K^* \to \pi K$ and $\phi K^* \to \pi K$ have comparable magnitude.

C. Resonance exchange in $\rho K^*, \omega K^*, \phi K^* \to \pi K$ through triangular loops

In addition to the mechanisms discussed so far to determine the cross sections of the reactions $\rho K^*, \omega K^*, \phi K^* \to \pi K$ (see Fig. 2), one could also consider the possibility of exchanging a resonance in the s channel, as in case of the $K_1(1270)$ exchange in πK^* collisions (see Fig. 1). Indeed,

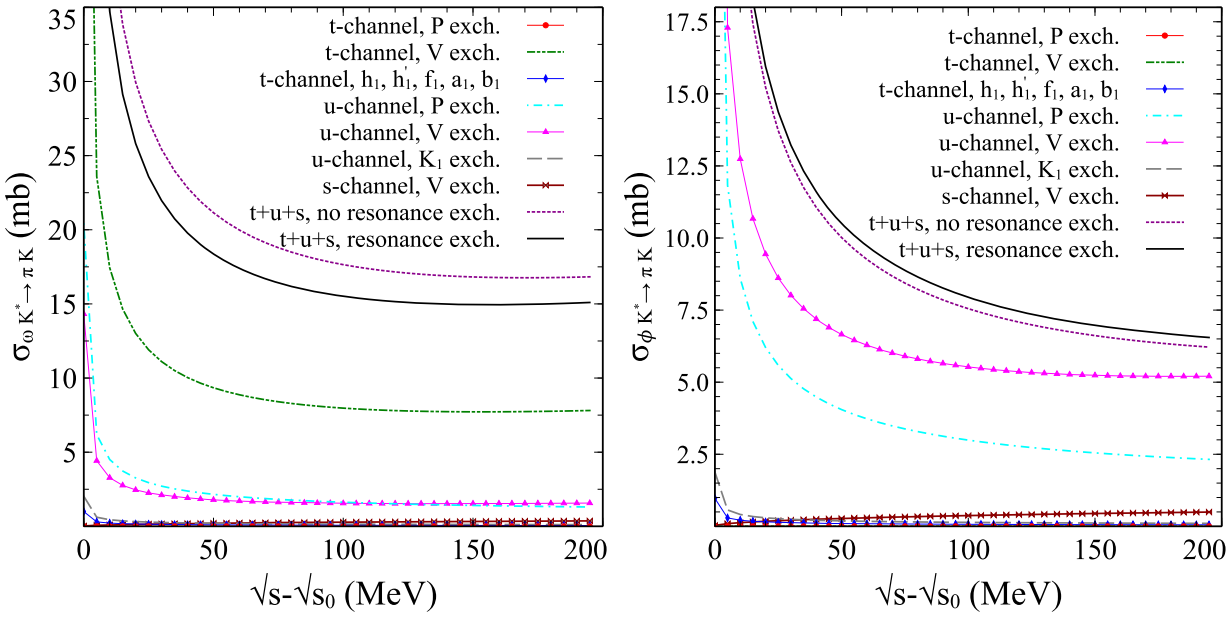

FIG. 6. Cross sections obtained with Eq. (1) for the processes $\omega K^* \to \pi K$ (left panel) and $\phi K^* \to \pi K$ (right panel) considering different mechanism as a function of $\sqrt{s} - \sqrt{s_0}$, where $\sqrt{s}$ is the center of mass energy and $\sqrt{s_0}$ is the threshold energy for the reaction. Since the cross section, independently of the mechanism, diverges at threshold, they have been calculated at an energy starting 0.5 MeV above the threshold of the reaction, so the x axis is actually $\sqrt{s} - \sqrt{s_0} + 0.5$ MeV. In the figure, $h_1 \equiv h_1(1170)$ and $h_1' \equiv h_1(1380)$. None of these processes were computed in Ref. [9].

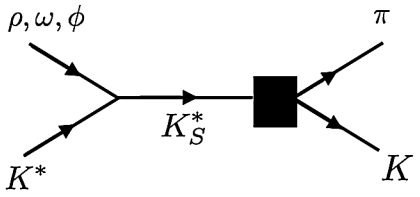

FIG. 7. Exchange of the K_S^* states found in Ref. [33] in the s channel for the reactions $\rho K^*, \omega K^*, \phi K^* \to \pi K$. The filled box in the figure corresponds to the vertex $K_S^* \pi K$, which is evaluated considering the triangular loop shown in Fig. 8.

in Ref. [33] the interaction of K^* with ρ, ω and ϕ in s-wave (orbital angular momentum 0) was investigated and several K^* resonances with $I = 1/2$ and different spin were found as a consequence of the dynamics involved: a $J^P = 0^+$ resonance with mass 1643 MeV and width of 48 MeV, which is a prediction of the theory; a 1^+ resonance with mass 1737 MeV and width of 164 MeV which is associated with the state $K_1^*(1650)$ listed by the PDG [13]; a $J^P = 2^+$ state with mass 1431 MeV and 56 MeV of width which is identified with the $K_2^*(1430)$ listed by the PDG. Thus, exchange of these K_S^* states (with S indicating the spin) in the s-channel, as shown in Fig. 7, can be important while calculating the cross section for $\rho K^* \to \pi K$. As can be seen in Fig. 7, one of the vertices involved in the process is the $K_S^* \pi K$ vertex. From Ref. [33], we have information on the pole positions of these K_S^* states and their couplings to the channels ρK^*, ωK^* and ϕK^* (which we list in Table XIII of Appendix B), but the couplings to two pseudoscalars are not available. However, in the model of Ref. [33] we can interpret the $K_S^* \pi K$ vertex as an effective one: due to the vector-vector dynamical nature of these K_S^* states, two pseudoscalar channels were not considered as a part of the coupled channel space in Ref. [33]. Within the approach of Ref. [33], the simplest way of considering K_S^* exchange in the s-channel is through an effective vertex, represented by a filled box in Fig. 7, which involves triangular loops (see Fig. 8). This is similar to the case of other molecular type resonances, like $X(3872)$, $N(1700) J^P = 3/2^-$, $f_1(1285)$, $a_1(1420)$, where the simplest mechanism to explain their decay modes is through triangular loops (see Refs. [16,34–37]).

The details related to the determination of the amplitude for the process depicted in Fig. 7 can be found in Appendix B. Since the interaction of the initial vector-vector system in the diagram of Fig. 7 would generate these K_S^* states, the quantum numbers for the external vectors system can be $J^P = 0^+, 1^+$ or 2^+. The final state in Fig. 7 consists of two pseudoscalars (total spin 0), thus, the only way of getting $J = 1$ is with one unit of orbital angular momentum which leads the two pseudoscalar system to have $J^P = 1^-$ instead of the initial 1^+. This means that in the diagram of Fig. 7 we can not have a transition in the s channel through the exchange of the K_1^* resonance found in Ref. [33]. Similarly, we can not have interference between the diagrams in Fig. 2(c), which involves the exchange of a pseudoscalar or vector meson (thus, a initial state having negative total parity), and the diagram in Fig. 7.

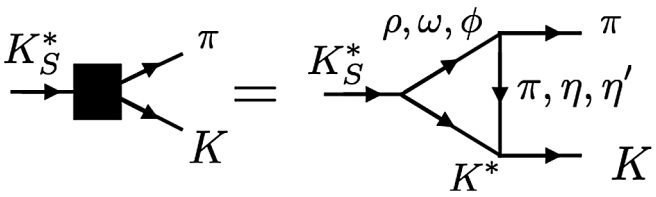

FIG. 8. The $K_S^* \pi K$ vertex.

In Fig. 9, we show the cross section for the process $\rho K^* \to \pi K$ considering s-channel exchange of the K_S^* resonances. As can be seen by comparing with the results shown in Fig. 5, the contribution to the cross section of the mechanism depicted in Fig. 7 is very relevant. These results suggest that the inclusion of the process shown in Fig. 7 must strongly affect the production of K^* and K in heavy ion collisions.

In Fig. 10, we show the results found for the cross section related to the s-channel exchange of K_S^* in case of the reactions $\omega K^* \to \pi K$ (left panel) and $\phi K^* \to \pi K$ (right panel). By comparing with the results found in Fig. 6, this mechanism also produces changes in the cross section obtained without the s-channel K_S^* exchange, although milder than in case of the reaction $\rho K^* \to \pi K$.

D. Cross sections for the inverse reactions

We can obtain the cross section for the production of K^* from the reactions $\rho K, \omega K, \phi K \to \pi K^*$ and $\pi K \to \rho K^*$,

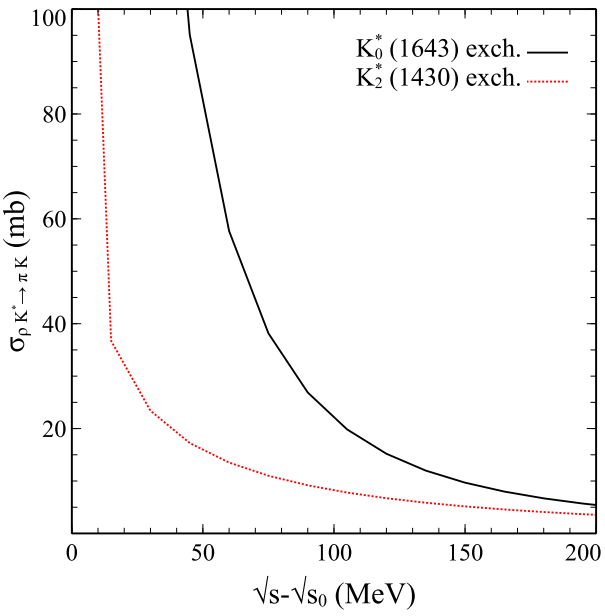

FIG. 9. Contribution to the cross section of $\rho K^* \to \pi K$ from the triangular loops shown in Fig. 8, in which we consider the exchange of the states listed in Table XIII.

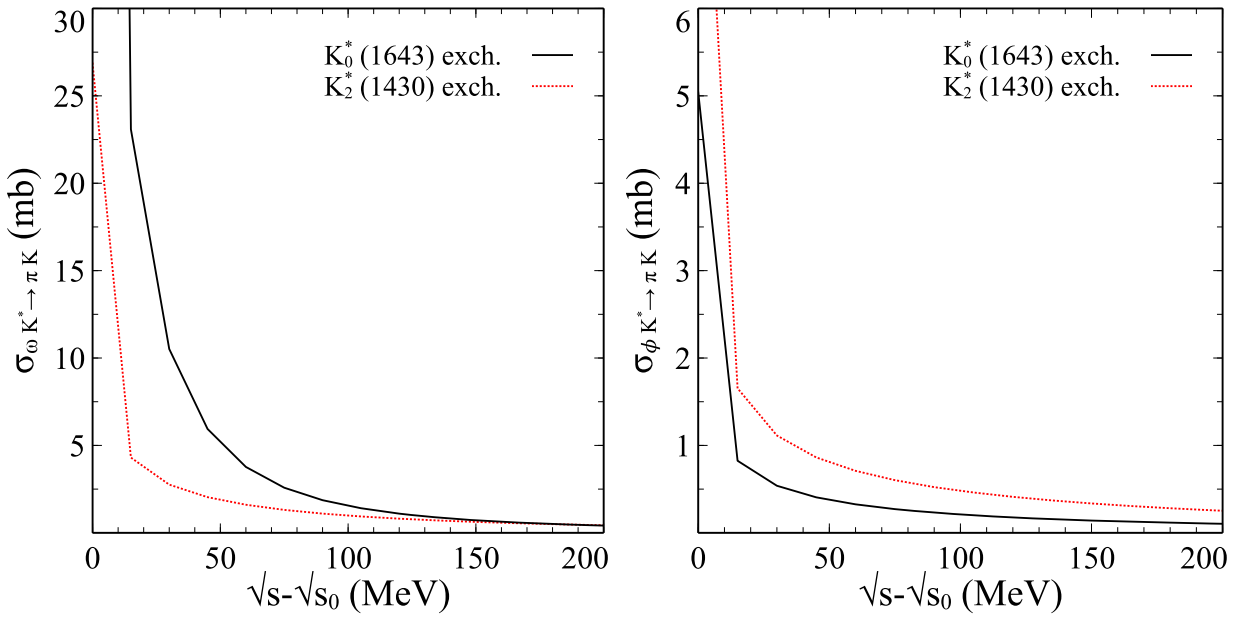

FIG. 10. Contribution to the cross section of $\omega K^* \to \pi K$ (left panel) and $\phi K^* \to \pi K$ (right panel) from the s-channel exchange of the K_S^* states listed in Table XIII.

$\omega K^*, \phi K^*$ using the principle of detailed balance: if $\sigma_{ab\to cd}$ is the cross section for the process $a + b \to c + d$, calculated via Eq. (1), we can determine the cross section for the inverse reaction, $c + d \to a + b$, as

$$\sigma_{cd\to ab} = \frac{(2s_a+1)(2s_b+1)(2I_a+1)(2I_b+1)}{(2s_c+1)(2s_d+1)(2I_c+1)(2I_d+1)} \times \frac{\lambda(s,m_a^2,m_b^2)}{\lambda(s,m_c^2,m_d^2)}\sigma_{ab\to cd}. \quad (18)$$

In Fig. 11, we show the results obtained for the K^* production cross sections using the principle of detailed balance. On the left panel, we show the cross sections found for $\rho K, \omega K, \phi K \to \pi K^*$ (thick lines) determined from the cross sections shown in Figs. 3, 4 (solid lines) and Eq. (18). The peak like structure found in the results for the reaction $\rho K \to \pi K^*$ corresponds to the manifestation of $K_1(1270)$. For the sake of comparison, we have also plotted the results found in Figs. 3, 4 for the cross sections of the K^* absorption in the reactions $\pi K^* \to \rho K, \omega K, \phi K$. On the right panel, we show the results found for the cross sections of the reactions $\pi K \to \rho K^*, \omega K^*, \phi K^*$, which have been determined by using the results obtained in Figs. 5, 6, 9, 10 (solid lines) and Eq. (18).

As can be seen in Fig. 11 (left panel), the absorption cross sections of K^* by π are smaller than the corresponding ones for the production processes through collisions of K with ρ, ω or ϕ. The trend is the same in case of the absorption of K^* by ρ for excitation energies above ~90 MeV (right panel), while the absorption cross sections of K^* by ω or ϕ are larger than those related to its production from collisions of π and K. However, for excitation energies bigger than ~90 MeV the cross section for the $\pi K \to \rho K^*$ process dominates above all.

Very recently, K and K^* formation in relativistic heavy-ion collisions has been investigated in the context of the Parton-Hadron-String dynamics (PHSD) transport approach [38,39], which considers the in-medium effects in the K and $\bar{K}^*$ states through the modification of their spectral properties during the propagation through the medium. The authors conclude that final state interactions (in the hadron gas) contribute to reduce the ratio K^*/K, corroborating the findings of Ref. [9].

In this latter model, the relevance of the absorption and production mechanisms of K^* and K mesons in the QGP to the abundances of K^* and K at the kinetic freeze-out temperature appears through the thermal average cross sections for such processes. These thermal averaged cross sections affect the time evolution of the abundance of K^* and K in the corresponding rate equations, where the quantity $\langle \sigma v_{\rm rel} \rangle$ enters as input in the equations (here the symbol $< >$ represents the thermal average and $v_{\rm rel}$ is the relative velocity between the particles present in the initial state of the process whose cross section is σ). Due to the relevance of the quantity $\langle \sigma v_{\rm rel} \rangle$, we present our results for the thermal averaged cross sections of Fig. 11 in the next section.

E. Thermal averaged cross sections

For a process $a + b \to c + d$, thermal averaged cross sections are given by [9,40],

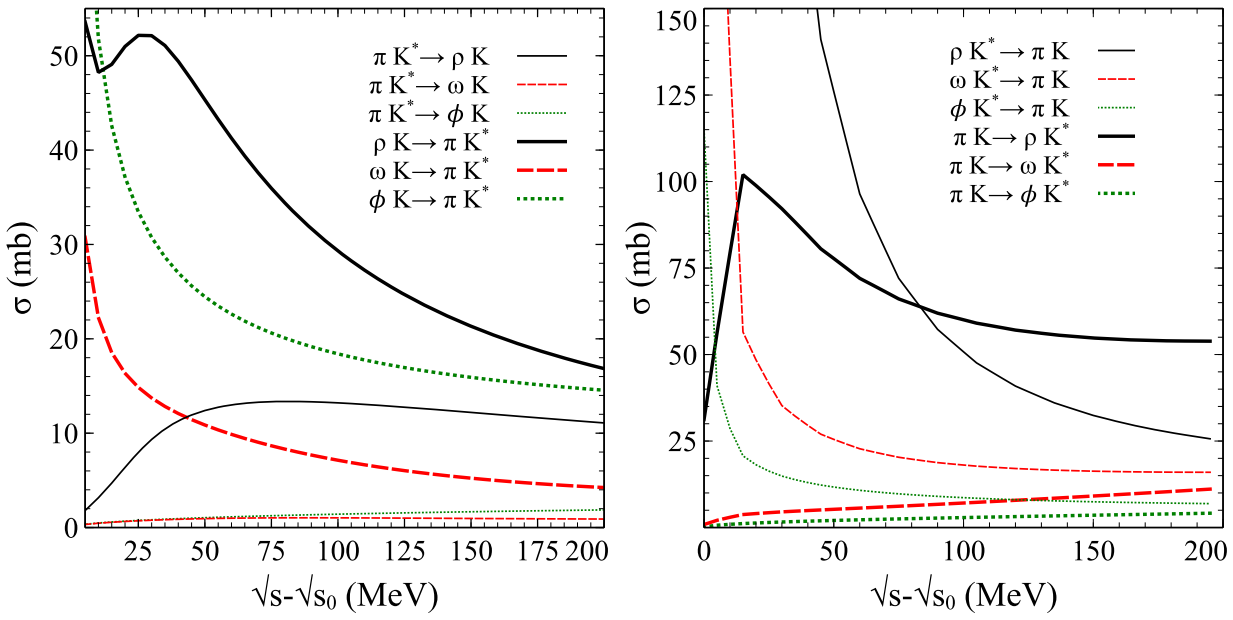

FIG. 11. Cross sections for $\pi K^* \leftrightarrow \rho K, \omega K, \phi K$ (left panel) and $\rho K^*, \omega K^*, \phi K^* \leftrightarrow \pi K$ (right panel).

$$\langle \sigma_{ab\to cd} v_{ab} \rangle = \frac{\int d^3p_a d^3p_b f_a(\vec{p}_a) f_b(\vec{p}_b) v_{ab} \sigma_{ab\to cd}}{\int d^3p_a d^3p_b f_a(\vec{p}_a) f_b(\vec{p}_b)} = \frac{1}{4\alpha_a^2 K_2(\alpha_a)\alpha_b^2 K_2(\alpha_b)} \int_{z_0}^{\infty} dz K_1(z) \sigma_{ab\to cd}(z) \times [z^2 - (\alpha_a + \alpha_b)^2][z^2 - (\alpha_a - \alpha_b)^2], \quad (19)$$

where $z = \sqrt{s}/T$, with T being the temperature of the medium, v_{ab} represents the relative velocity between particles a and b, $f_i(\vec{p}_i)$ is the Boltzmann momentum distribution of particle i with momentum $\vec{p}_i$, $\alpha_i = m_i/T$, with m_i being the mass of particle i, $z_0 = \max(\alpha_a + \alpha_b, \alpha_c + \alpha_d)$, and $K_1(z)$ and $K_2(z)$ are the modified Bessel functions of the second kind, of order 1 and 2, respectively.

In Fig. 12, we show the thermal averaged cross sections for the results shown in Fig. 11. As can be seen, the thermal averaged cross sections for K^* production from collisions of ρ, ω and ϕ with kaons are larger than the corresponding K production cross sections from collisions of π with K^* (see the left panel of Fig. 12). On the contrary, the K production cross sections from the collision of ρ, ω and ϕ

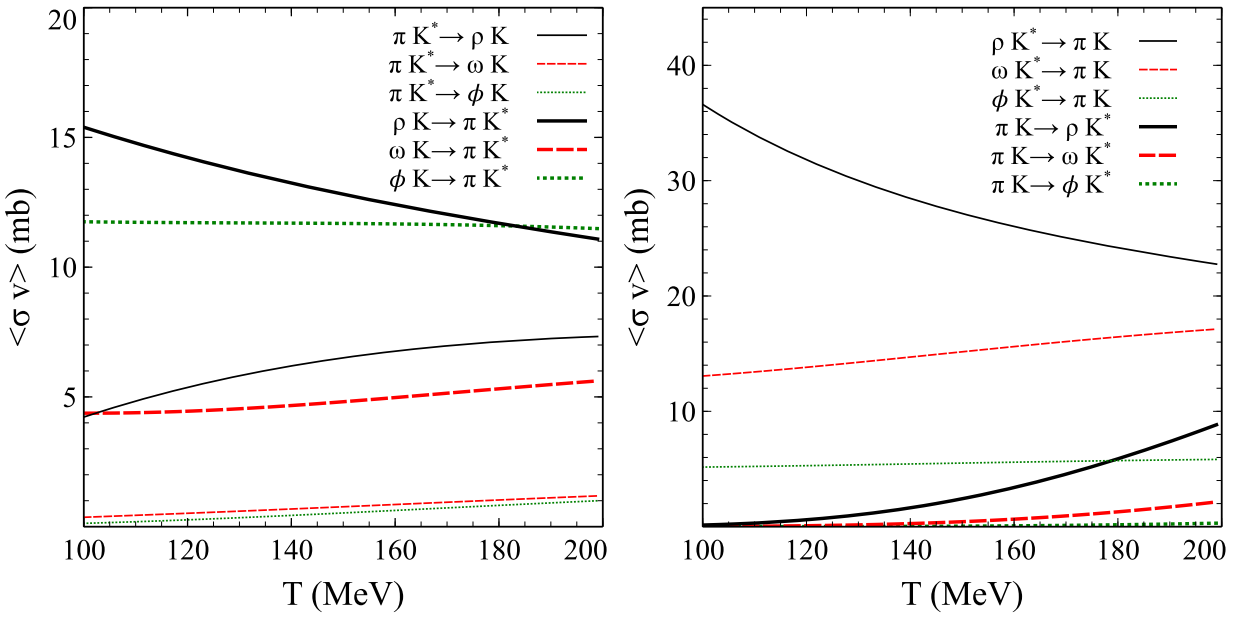

FIG. 12. Thermal averaged cross sections for $\pi K^* \leftrightarrow \rho K, \omega K, \phi K$ (left panel) and $\rho K^*, \omega K^*, \phi K^* \leftrightarrow \pi K$ (right panel).

with K^* are larger than those related to the K^* production from collisions between π and K (see the right panel of Fig. 12). The largest of all is the production cross section of K from the $\rho - K^*$ collisions, throughout the range of the temperature shown in Fig. 12. On the other hand, the largest cross section for the K^* production come from $\rho - K$ collisions, which when compared with the former is about a factor two smaller. Whether this is or not an indication of a possible K^* suppression of the K^* yield in a pos-QGP hadronic medium can only be disentangled by solving the rate equations for the abundances of K and K^*, in which the number of π, ρ, ω, ϕ, K, K^* present in the medium would also play a crucial role in determining which of the processes shown in Fig. 12 turns to dominate, if any. A detailed analysis based on the study of the rate equations is in progress and will be published soon.

IV. CONCLUSIONS

We have determined the cross sections related to the processes $\pi K^* \to \rho K$, $\omega K \phi K$ and ρK^*, $\omega K^* \phi K^* \to \pi K$ considering the exchange of pseudoscalars, vectors and several resonances. The reactions $\pi K^* \to \rho K$ and $\rho K^* \to \pi K$, together with $K^* \to K\pi$, $K\pi \to K^*$, were found in Ref. [9] to be the reactions contributing dominantly to the abundance ratio of K^* and K in heavy ion collisions. However, several mechanisms which could contribute to the cross sections of $\pi K^* \to \rho K$ and $\rho K^* \to \pi K$ were missing in Ref. [9]. With the purpose of obtaining information on such processes, we consider a more complete formalism, which takes into account more mechanisms and calculate cross sections. We find that some of these new contributions turn out to be especially important, as the pseudoscalar exchange in the t channel for the processes $\pi K^* \to \rho K$ and $\rho K^* \to \pi K$, exchange of resonances in the s channel, like $K_2^*(1430)$, for $\rho K^* \to \pi K$, etc. We have also determined the cross sections for the inverse processes using the principle of detailed balance. To present a more summarized picture, we have given the thermal averaged cross sections. The comparison between the direct and inverse processes shown in Fig. 12 shows that the production of K from ρK^* collisions gives the largest thermal averaged cross section in all the range of temperatures. Whether this dominance translates or not to a suppression of the K^* yield measured in heavy ion collisions can be known by solving the rate equations for the abundances of K and K^* and their time evolution. Our results should be useful in obtaining a more accurate time evolution for the abundance ratio of K^* and K in heavy ion collisions.

ACKNOWLEDGMENTS

The authors would like to thank the Brazilian funding agencies FAPESP (under the Grant No. 2012/50984-4) and CNPq for the financial support (under the Grants No. 310759/2016-1 and No. 311524/2016-8).

APPENDIX A: INFORMATION RELATED TO THE EXCHANGED RESONANCES IN THE t, u AND s CHANNELS

In Tables I and II of this appendix, we list, for completeness, the pole positions and couplings of the states found in Refs. [10,11]. These couplings are in the isospin base and to determine their values in the charge

TABLE I. Pole positions and couplings of the $K_1(1270)$ state to the different coupled channels whose dynamics generates the state [10,11]. A two pole structure is found for $K_1(1270)$ in Refs. [10,11] and the values shown in this table have been taken from Ref. [11]. The pole positions written in the table corresponds to $M - i\frac{\Gamma}{2}$, with M and Γ the mass and width characterizing the state. The numerical values for the masses, widths and couplings of the states are expressed in MeV.

Pole	$1195 - i123$	$1284 - i73$
Channel	Coupling constant	
ϕK	$2096 - i1208$	$1166 - i774$
ωK	$-2046 + i821$	$-1051 + i620$
ρK	$-1671 + i1599$	$4804 + i395$
$K^*\eta$	$72 + i197$	$3486 - i536$
$K^*\pi$	$4747 - i2874$	$769 - i1171$

TABLE II. Pole positions and couplings of the axial resonances $h_1(1170)$, $h_1(1380)$ (strangeness $S=0$, isospin $I=0$, G-parity $G=-$), $f_1(1285)$ ($S=0$, $I=0$, $G=+$), $a_1(1260)$ ($S=0$, $I=1$, $G=-$) and $b_1(1235)$ ($S=0$, $I=1$, $G=+$) to the different coupled channels whose dynamics generates them [10]. The values shown in this table have been taken from Ref. [10]. The pole positions written in the table corresponds to $M - i\frac{\Gamma}{2}$, with M and Γ the mass and width characterizing the state. The numerical values for the masses, widths and couplings of the states are expressed in MeV.

State ($G=-$)	$h_1(1170)$	$h_1(1380)$	$a_1(1260)$
Pole	$919 - i17$	$1245 - i7$	$1011 - i84$
Channel ($G=-$)	Coupling constant		
$\frac{1}{\sqrt{2}}[\bar{K}^*K - K^*\bar{K}]$	$781 - i498$	$6147 + i183$	$1872 - i1486$
$\phi\eta$	$46 - i13$	$-3311 + i47$	0
$\omega\eta$	$23 - i28$	$3020 - i22$	0
$\rho\pi$	$-3453 + i1681$	$648 - i959$	$-3795 + i2330$

State ($G=+$)	$f_1(1285)$	$b_1(1235)$
Pole	$1288 - i0$	$1245 - i28$
Channel ($G=+$)	Coupling constant	
$\frac{1}{\sqrt{2}}[\bar{K}^*K + K^*\bar{K}]$	$7230 + i0$	$6172 - i75$
$\phi\pi$	0	$2087 - i385$
$\omega\pi$	0	$-1869 + i300$
$\rho\eta$	0	$-3041 + i498$

TABLE III. Coefficients $\mathbb{T}_k^{ij}$ present in Eq. (9) for the reactions $r = \pi K^* \to \rho K, \omega K, \phi K$ for total charge -1, 0, 1 and 2. The index i represents the initial state πK^* for a particular charge configuration and the index j corresponds to the final state for the same total charge. The index k corresponds to the exchanged pseudoscalar, which we indicate in brackets next to the coefficient. The absence of the coefficient for some k means that the coefficient is 0 for that exchanged particle. If no exchanged particle is indicated next to the coefficient, the coefficient is 0 independently of the exchanged particle.

				$\rho^- K^0$
$\pi^- K^{*0}$				$4(\pi^0)$

	$\rho^- K^+$	$\rho^0 K^0$	ωK^0	ϕK^0
$\pi^- K^{*+}$	$-4(\pi^0)$	$4\sqrt{2}(\pi^-)$	0	0
$\pi^0 K^{*0}$	$4\sqrt{2}(\pi^+)$	0	0	0

				$\rho^+ K^+$
$\pi^+ K^{*+}$				$4(\pi^0)$

	$\rho^0 K^+$	$\rho^+ K^0$	ωK^+	ϕK^+
$\pi^0 K^{*+}$	0	$-4\sqrt{2}(\pi^-)$	0	0
$\pi^+ K^{*0}$	$-4\sqrt{2}(\pi^+)$	$-4(\pi^0)$	0	0

basis we use the Clebsch-Gordan coefficients and the following convention to associate particles with states in the isospin base $|I, I_3\rangle$ (with I being the total isospin and I_3 its third projection)

TABLE IV. Coefficients $\bar{\mathbb{T}}_k^{ij}$ present in Eq. (9) for the reactions $r = \pi K^* \to \rho K, \omega K, \phi K$ for total charge -1, 0, 1 and 2. The index i represents the initial state πK^* for a particular charge configuration and the index j corresponds to the final state for the same total charge. The index k corresponds to the exchanged vector, which we indicate in brackets next to the coefficient. See the caption of Table III for the notation used here.

				$\rho^- K^0$
$\pi^- K^{*0}$				$-\frac{1}{2}(\omega)$

	$\rho^- K^+$	$\rho^0 K^0$	ωK^0	ϕK^0
$\pi^- K^{*+}$	$-\frac{1}{2}(\omega)$	0	$-\frac{1}{\sqrt{2}}(\rho^-)$	0
$\pi^0 K^{*0}$	0	$-\frac{1}{2}(\omega)$	$\frac{1}{2}(\rho^0)$	0

				$\rho^+ K^+$
$\pi^+ K^{*+}$				$-\frac{1}{2}(\omega)$

	$\rho^0 K^+$	$\rho^+ K^0$	ωK^+	ϕK^+
$\pi^0 K^{*+}$	$-\frac{1}{2}(\omega)$	0	$-\frac{1}{2}(\rho^0)$	0
$\pi^+ K^{*0}$	0	$-\frac{1}{2}(\omega)$	$-\frac{1}{\sqrt{2}}(\rho^+)$	0

TABLE V. Coefficients $\mathbb{U}_k^{ij}$ present in Eq. (10) for the reactions $r = \pi K^* \to \rho K, \omega K, \phi K$ for total charge -1, 0, 1 and 2. See the caption of Table IV for the notation used here.

				$\rho^- K^0$
$\pi^- K^{*0}$				$1(K^{*-})$

	$\rho^- K^+$	$\rho^0 K^0$	ωK^0	ϕK^0
$\pi^- K^{*+}$	0	$\frac{1}{\sqrt{2}}(K^{*-})$	$\frac{1}{\sqrt{2}}(K^{*-})$	$-1(K^{*-})$
$\pi^0 K^{*0}$	$\frac{1}{\sqrt{2}}(K^{*-})$	$\frac{1}{2}(\bar{K}^{*0})$	$-\frac{1}{2}(\bar{K}^{*0})$	$\frac{1}{\sqrt{2}}(\bar{K}^{*0})$

				$\rho^+ K^+$
$\pi^+ K^{*+}$				$1(\bar{K}^{*0})$

	$\rho^0 K^+$	$\rho^+ K^0$	ωK^+	ϕK^+
$\pi^0 K^{*+}$	$\frac{1}{2}(K^{*-})$	$-\frac{1}{\sqrt{2}}(\bar{K}^{*0})$	$\frac{1}{2}(K^{*-})$	$-\frac{1}{\sqrt{2}}(K^{*-})$
$\pi^+ K^{*0}$	$-\frac{1}{\sqrt{2}}(\bar{K}^{*0})$	0	$\frac{1}{\sqrt{2}}(\bar{K}^{*0})$	$-1(\bar{K}^{*0})$

$$|K^-\rangle = -\left|\frac{1}{2}, -\frac{1}{2}\right\rangle, \qquad |K^{*-}\rangle = -\left|\frac{1}{2}, -\frac{1}{2}\right\rangle,$$
$$|\pi^+\rangle = -|1, 1\rangle, \qquad |\rho^+\rangle = -|1, 1\rangle. \tag{A1}$$

In this way, for example, from Table II, we have that the coupling of the isospin 0, G-parity positive, state $f_1(1285)$ to $\frac{1}{\sqrt{2}}[\bar{K}^* K + K^* \bar{K}]$ (which corresponds to a positive G-parity combination) is $g = 7230 + i0$. This means that the state $f_1(1285)$ couples to the combination

TABLE VI. Coefficients $\mathbb{S}_K^{ij}$ present in Eq. (11) for the reactions $r = \pi K^* \to \rho K, \omega K, \phi K$ for total charge -1, 0, 1 and 2. In this case, a K^0 is exchanged for those processes whose total charge is 0 and a K^+ for total charge $+1$. For total charge -1 and 2, no particle can be exchanged in the s channel.

				$\rho^- K^0$
$\pi^- K^{*0}$				0

	$\rho^- K^+$	$\rho^0 K^0$	ωK^0	ϕK^0
$\pi^- K^{*+}$	-4	$2\sqrt{2}$	$-2\sqrt{2}$	4
$\pi^0 K^{*0}$	$2\sqrt{2}$	-2	2	$-2\sqrt{2}$

				$\rho^+ K^+$
$\pi^+ K^{*+}$				0

	$\rho^0 K^+$	$\rho^+ K^0$	ωK^+	ϕK^+
$\pi^0 K^{*+}$	-2	$-2\sqrt{2}$	-2	$2\sqrt{2}$
$\pi^+ K^{*0}$	$-2\sqrt{2}$	-4	$-2\sqrt{2}$	4

TABLE VII. Coefficients $\mathbb{S}^{ij}_{K^*}$ present in Eq. (11) for the reactions $r = \pi K^* \to \rho K, \omega K, \phi K$ for total charge −1, 0, 1 and 2. In this case, a K^{*0} is exchanged for those processes whose total charge is 0 and a K^{*+} for total charge +1. In case of total charge −1 and 2, no particle can be exchanged in the s channel.

	$\rho^- K^0$
$\pi^- K^{*0}$	0

	$\rho^- K^+$	$\rho^0 K^0$	ωK^0	ϕK^0
$\pi^- K^{*+}$	$-\frac{1}{2}$	$\frac{1}{2\sqrt{2}}$	$-\frac{1}{2\sqrt{2}}$	$-\frac{1}{2}$
$\pi^0 K^{*0}$	$\frac{1}{2\sqrt{2}}$	$-\frac{1}{4}$	$\frac{1}{4}$	$\frac{1}{2\sqrt{2}}$

	$\rho^+ K^+$
$\pi^+ K^{*+}$	0

	$\rho^0 K^+$	$\rho^+ K^0$	ωK^+	ϕK^+
$\pi^0 K^{*+}$	$-\frac{1}{4}$	$-\frac{1}{2\sqrt{2}}$	$-\frac{1}{4}$	$-\frac{1}{2\sqrt{2}}$
$\pi^+ K^{*0}$	$-\frac{1}{2\sqrt{2}}$	$-\frac{1}{2}$	$-\frac{1}{2\sqrt{2}}$	$-\frac{1}{2}$

$$\frac{1}{\sqrt{2}}[|\bar{K}^* K, I=0, I_3=0\rangle + |K^* \bar{K}, I=0, I_3=0\rangle] = \frac{1}{2}[|\bar{K}^{*0} K^0\rangle + |K^{*-} K^+\rangle - |K^{*+} K^-\rangle - |K^{*0} \bar{K}^0\rangle],$$

from which we get

TABLE VIII. Coefficients $\mathcal{T}^{ij}$ present in Eq. (15) for the reactions $r = \rho K^*, \omega K^*, \phi K^* \to \pi K$ for total charge −1, 0, 1 and 2. In this case, a vector meson is exchanged and we write the exchanged particle next to the coefficient. If the coefficient is 0, the process cannot proceed via vector meson exchange.

	$\pi^- K^0$
$\rho^- K^{*0}$	$4(\pi^0)$

	$\pi^- K^+$	$\pi^0 K^0$
$\rho^- K^{*+}$	$-4(\pi^0)$	$4\sqrt{2}(\pi^-)$
$\rho^0 K^{*0}$	$4\sqrt{2}(\pi^+)$	0
ωK^{*0}	0	0
ϕK^{*0}	0	0

	$\pi^+ K^+$
$\rho^+ K^{*+}$	$4(\pi^0)$

	$\pi^0 K^+$	$\pi^+ K^0$
$\rho^0 K^{*+}$	0	$-4\sqrt{2}(\pi^-)$
$\rho^+ K^{*0}$	$-4\sqrt{2}(\pi^+)$	$-4(\pi^0)$
ωK^{*+}	0	0
ϕK^{*+}	0	0

TABLE IX. Coefficients $\bar{\mathcal{T}}^{ij}$ present in Eq. (15) for the reactions $r = \rho K^*, \omega K^*, \phi K^* \to \pi K$ for total charge −1, 0, 1 and 2. See the caption of Table VIII for the notation used here.

	$\pi^- K^0$
$\rho^- K^{*0}$	$-\frac{1}{2}(\omega)$

	$\pi^- K^+$	$\pi^0 K^0$
$\rho^- K^{*+}$	$-\frac{1}{2}(\omega)$	0
$\rho^0 K^{*0}$	0	$-\frac{1}{2}(\omega)$
ωK^{*0}	$-\frac{1}{\sqrt{2}}(\rho^+)$	$\frac{1}{2}(\rho^0)$
ϕK^{*0}	0	0

	$\pi^+ K^+$
$\rho^+ K^{*+}$	$-\frac{1}{2}(\omega)$

	$\pi^0 K^+$	$\pi^+ K^0$
$\rho^0 K^{*+}$	$-\frac{1}{2}(\omega)$	0
$\rho^+ K^{*0}$	0	$-\frac{1}{2}(\omega)$
ωK^{*+}	$-\frac{1}{2}(\rho^0)$	$-\frac{1}{\sqrt{2}}(\rho^-)$
ϕK^{*+}	0	0

$$g_{f_1 \to \bar{K}^{*0} K^0} = g_{f_1 \to K^{*-} K^+} = -g_{f_1 \to K^{*+} K^-} = -g_{f_1 \to K^{*0} \bar{K}^0} = \frac{1}{2} g. \tag{A2}$$

In Tables III–XII, we give the coefficients entering in the t-, u- and s- channel amplitudes of Figs. 1 and 2.

TABLE X. Coefficients $\mathcal{U}^{ij}_{\bar{K}}$ present in Eq. (16) for the reactions $r = \rho K^*, \omega K^*, \phi K^* \to \pi K$ for total charge −1, 0, 1 and 2. In this case, a $\bar{K}$ meson is exchanged in all diagrams.

	$\pi^- K^0$
$\rho^- K^{*0}$	4

	$\pi^- K^+$	$\pi^0 K^0$
$\rho^- K^{*+}$	0	$2\sqrt{2}$
$\rho^0 K^{*0}$	$2\sqrt{2}$	2
ωK^{*0}	$2\sqrt{2}$	−2
ϕK^{*0}	−4	$2\sqrt{2}$

	$\pi^+ K^+$
$\rho^+ K^{*+}$	4

	$\pi^0 K^+$	$\pi^+ K^0$
$\rho^0 K^{*+}$	2	$-2\sqrt{2}$
$\rho^+ K^{*0}$	$-2\sqrt{2}$	0
ωK^{*+}	2	$2\sqrt{2}$
ϕK^{*+}	$-2\sqrt{2}$	−4

TABLE XI. Coefficients $\mathcal{U}^{ij}_{\bar{K}^*}$ present in Eq. (16) for the reactions $r = \rho K^*, \omega K^*, \phi K^* \to \pi K$ for total charge -1, 0, 1 and 2. In this case, a $\bar{K}^*$ meson is exchanged in all diagrams.

		$\pi^- K^0$
$\rho^- K^{*0}$		$-\frac{1}{2}$

	$\pi^- K^+$	$\pi^0 K^0$
$\rho^- K^{*+}$	0	$-\frac{1}{2\sqrt{2}}$
$\rho^0 K^{*0}$	$-\frac{1}{2\sqrt{2}}$	$-\frac{1}{4}$
ωK^{*0}	$-\frac{1}{2\sqrt{2}}$	$\frac{1}{4}$
ϕK^{*0}	$-\frac{1}{2}$	$\frac{1}{2\sqrt{2}}$

		$\pi^+ K^+$
$\rho^+ K^{*+}$		$-\frac{1}{2}$

	$\pi^0 K^+$	$\pi^+ K^0$
$\rho^0 K^{*+}$	$-\frac{1}{4}$	$\frac{1}{2\sqrt{2}}$
$\rho^+ K^{*0}$	$\frac{1}{2\sqrt{2}}$	0
ωK^{*+}	$-\frac{1}{4}$	$-\frac{1}{2\sqrt{2}}$
ϕK^{*+}	$-\frac{1}{2\sqrt{2}}$	$-\frac{1}{2}$

TABLE XII. Coefficients $\mathcal{S}^{ij}$ present in Eq. (17) for the reactions $r = \rho K^*, \omega K^*, \phi K^* \to \pi K$ for total charge -1, 0, 1 and 2. In this case, a $\bar{K}^*$ meson is exchanged in all diagrams.

		$\pi^- K^0$
$\rho^- K^{*0}$		0

	$\pi^- K^+$	$\pi^0 K^0$
$\rho^- K^{*+}$	1	$-\frac{1}{\sqrt{2}}$
$\rho^0 K^{*0}$	$-\frac{1}{\sqrt{2}}$	$\frac{1}{2}$
ωK^{*0}	$\frac{1}{\sqrt{2}}$	$-\frac{1}{2}$
ϕK^{*0}	-1	$\frac{1}{\sqrt{2}}$

		$\pi^+ K^+$
$\rho^+ K^{*+}$		0

	$\pi^0 K^+$	$\pi^+ K^0$
$\rho^0 K^{*+}$	$\frac{1}{2}$	$\frac{1}{\sqrt{2}}$
$\rho^+ K^{*0}$	$\frac{1}{\sqrt{2}}$	1
ωK^{*+}	$\frac{1}{2}$	$\frac{1}{\sqrt{2}}$
ϕK^{*+}	$-\frac{1}{\sqrt{2}}$	-1

TABLE XIII. Pole positions and couplings of the vector resonances $K_0^*(1643)$ ($I = 1/2$, spin 0) and $K_2^*(1430)$ ($I = 1/2$, spin 2) found in Ref. [33], with the former being a prediction of the model. The pole positions written in the table corresponds to $M - i\frac{\Gamma}{2}$, with M and Γ the mass and width characterizing the state. The numerical values for the masses, widths and couplings of the states are expressed in MeV.

State	$K_0^*(1643)$	$K_2^*(1430)$
Pole	$1643 - i24$	$1431 - i28$
Channel	Coupling constant	
ρK^*	$8102 - i959$	$10901 - i71$
ωK^*	$1370 - i146$	$2267 - i13$
ϕK^*	$-1518 + i209$	$-2898 + i17$

APPENDIX B: EVALUATION OF THE s-CHANNEL EXCHANGE OF RESONANCES IN THE REACTIONS $\rho K^*, \omega K^*, \phi K^* \to \pi K$

In this appendix, we determine the amplitude related to the process depicted in Fig. 7 in which the K_S^* states (where the subscript S indicates spin) found in Ref. [33] are exchanged in the s channel through triangular loops (see Fig. 8). We have summarized the properties found in Ref. [33] for these K_S^* in Table XIII.

We have the following expression for the amplitude of the process depicted in Fig. 7

$$\boldsymbol{S}^{ij}_{K_S^*} = \sum_{k_1,k_2,k_3} g^{(i)}_{K_S^*} g^{(k_1k_2)}_{K_S^*} \frac{1}{s - M^2_{K_S^*} + i\Gamma_{K_S^*} M_{K_S^*}} \times g^2_{PPV} \mathcal{S}^{(k_1k_2k_3)} P_S^{\mu\nu} p'_\mu I_\nu^{(k_1k_2k_3)}, \tag{B1}$$

where the coefficients $\mathcal{S}^{(k_1k_2k_3)}$ are given in Table XIV. The symbols $M_{K_S^*}$ and $\Gamma_{K_S^*}$ in Eq. (B1) are the mass and width of the poles related to the exchanged K_S^* state, while $g^{(i)}_{K_S^*}$ and $g^{(k_1k_2)}_{K_S^*}$ are, respectively, the coupling constants of those poles to the initial state and to the vector mesons present in

TABLE XIV. Coefficients $\mathcal{S}^{(k_1k_2k_3)}$ present in Eq. (B1) for the reactions $r = \rho K^*, \omega K^*, \phi K^* \to \pi K$ for total charge -1, 0, 1 and 2. We indicate those particles (related to the indices k_1, k_2 and k_3) which, when involved in the triangular loop, give a nonzero coefficient.

$(k_1k_2k_3)$	$\mathcal{S}^{(k_1k_2k_3)}$
$\rho^- K^{*+} \pi^0$	2
$\rho^0 K^{*0} \pi^+$	$-2\sqrt{2}$
$\rho^- K^{*+} \pi^-$	$-2\sqrt{2}$
$\rho^+ K^{*0} \pi^+$	$2\sqrt{2}$
$\rho^0 K^{*+} \pi^-$	$2\sqrt{2}$
$\rho^+ K^{*0} \pi^0$	2

the triangular loops shown in Fig. 8. The numerical values for these quantities can be found in Table XIII.

To get Eq. (B1), we have used the following amplitude for the coupling of the K_S^* states to the vector mesons

$$t_{K_S^*} = g^{(i)}_{K_S^*} g^{(k_1 k_2)}_{K_S^*} \frac{1}{s - M^2_{K_S^*} + i\Gamma_{K_S^*} M_{K_S^*}} P_S, \tag{B2}$$

where P_S is a spin projector, which is given for the case of spin $S = 0,\ 2$ by [41]

$$\begin{aligned} P_0 &= \frac{1}{3}\epsilon_\mu(k)\epsilon^\mu(p)\epsilon_\nu(q)\epsilon^\nu(p+k-q), \\ P_2 &= \frac{1}{2}[\epsilon_\mu(p)\epsilon_\nu(k)\epsilon^\mu(q)\epsilon^\nu(p+k-q) \\ &\quad + \epsilon_\mu(p)\epsilon_\nu(k)\epsilon^\nu(q)\epsilon^\mu(p+k-q)] \\ &\quad - \frac{1}{3}\epsilon_\alpha(p)\epsilon^\alpha(k)\epsilon_\beta(q)\epsilon^\beta(p+k-q). \end{aligned} \tag{B3}$$

In Eq. (B3), q and $p+k-q$ represent, respectively, the four momenta of the vector meson without strangeness and the K^* meson present in the triangular loop of Fig. 8 and which are coupled to K_S^*.

Since K_S^* can be considered as molecular state of ρK^* and coupled channels [33] with its hadron components being in s-wave, the vector mesons present in the triangular loops and which couple to K_S^*, although being off-shell, should not be very far from being on-shell (i.e., their respective modulus of the three-momenta are negligible as compared to their energies). Within such an interpretation of K_S^*, the temporal part of the polarization vectors ($\sim$ modulus of momentum divided by mass) of the mesons at the resonance-meson-meson vertex should be negligible as compared to the spatial components. This means that for the external as well as the internal vector mesons coupled to K_S^* we can use the approximation [33,41]

$$\sum_{\text{polarizations}} \epsilon^\mu \epsilon^\nu \sim \sum_{\text{polarizations}} \epsilon^i \epsilon^j = \delta^{ij}, \tag{B4}$$

with i and j being spatial indices. However, it would be more appropriate to maintain the covariant formalism instead of working with mixed indices (some spatial and other temporal-spatial). This can be achieved by writting

$$\sum_{\text{polarizations}} \epsilon^\mu \epsilon^\nu \sim -g^{\mu\nu}, \tag{B5}$$

for the vector mesons coupled to K_S^* present in the triangular loop of Fig. 8. This approximation implies the inclusion, in the result, of a very small contribution arising from the temporal part of the polarization vector of these vector mesons. We have made use of this approximation to get Eq. (B1). When summing over the polarizations of the external vector mesons coupled to K_S^* we use

$$\begin{aligned} \sum_{\text{polarizations}} \epsilon^\mu(k)\epsilon^\nu(k) &= -g^{\mu\nu} + \frac{k^\mu k^\nu}{m^2_{K^*}}, \\ \sum_{\text{polarizations}} \epsilon^\mu(p)\epsilon^\nu(p) &= -g^{\mu\nu} + \frac{p^\mu p^\nu}{m^2_V}, \end{aligned} \tag{B6}$$

which will produce negligible values for the temporal and temporal-spatial components. This is so because, as mentioned above, the external vectors, when interacting in s-wave and for energies not far away from the threshold (as in our case), generate the K_S^* (following the interpretation of Ref. [33]). Thus, the modulus of their momenta is much smaller than their energies, so

$$\begin{aligned} \sum_{\text{polarizations}} \epsilon^0(k)\epsilon^0(k) &= -g^{00} + \frac{k^0 k^0}{m^2_{K^*}} = -1 \\ &\quad + \frac{k^0 k^0}{m^2_{K^*}} \sim -1 + 1 = 0, \\ \sum_{\text{polarizations}} \epsilon^i(k)\epsilon^0(k) &= -g^{i0} + \frac{k^i k^0}{m^2_{K^*}} = \frac{k^i k^0}{m^2_{K^*}} \sim 0, \\ \sum_{\text{polarizations}} \epsilon^i(k)\epsilon^j(k) - g^{ij} + \frac{k^i k^j}{m^2_{K^*}} &= 1 + \frac{k^i k^j}{m^2_{K^*}} \sim 1, \end{aligned} \tag{B7}$$

and the same is the case for $\epsilon(p)$. Then, the use of Eqs. (B5) and (B6) is in line with the approximation in Eq. (B4).

The summation over the polarizations of the vector mesons in the triangular loop coupled to K_S^* gives rise to the $P_S^{\mu\nu}$ present in Eq. (B1), which is a spin projector for the external vector mesons coupled to K_S^*. Within the approximation of Eqs. (B5) and (B6), we have for spin $S = 0,\ 2$

$$\begin{aligned} P_0^{\mu\nu} &= \frac{1}{3}\epsilon(p)\cdot\epsilon(k) g^{\mu\nu}, \\ P_2^{\mu\nu} &= \frac{1}{2}[\epsilon^\mu(p)\epsilon^\nu(k) + \epsilon^\nu(p)\epsilon^\mu(k)] - \frac{1}{3}\epsilon(p)\cdot\epsilon(k) g^{\mu\nu}. \end{aligned} \tag{B8}$$

These expressions can be compared with the spin projectors found in Ref. [41] for the case of spatial indices and neglecting the temporal part of the polarization vector,

$$\begin{aligned} P_0^{ij} &= \frac{1}{3}\vec{\epsilon}(p)\cdot\vec{\epsilon}(k)\delta^{ij}, \\ P_2^{ij} &= \frac{1}{2}[\epsilon^i(p)\epsilon^j(k) + \epsilon^j(p)\epsilon^i(k)] - \frac{1}{3}\vec{\epsilon}(p)\cdot\vec{\epsilon}(k)\delta^{ij}. \end{aligned} \tag{B9}$$

In this case, Eq. (B4) is used to sum over the polarizations.

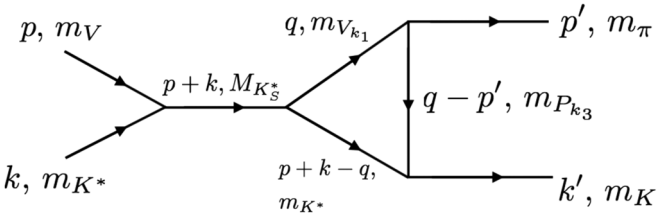

FIG. 13. Momentum and mass assignations for the particles involved in the triangular loop diagram of Fig. 8. The mass m_V is associated with the external ρ, ω or ϕ mesons; $m_{V_{k_1}}$ and $m_{V_{k_2}} = m_{K^*}$ are the masses of the vector mesons which can couple to K_S^* and they are listed in Table XIII. The mass $m_{P_{k_3}}$ is related to the pseudoescalars (π, η, η') which can be exchanged.

In Eq. (B1), $I_\nu^{(k_1k_2k_3)}$ corresponds to the following integral

$$I_\nu^{(k_1k_2k_3)} = \int \frac{d^4q}{(2\pi)^4}\frac{1}{q^2 - m_{V_{k_1}}^2 + i\epsilon} \times \frac{(k' - p' + q)_\nu}{(p + k - q)^2 - m_{V_{k_2}}^2 + i\epsilon} \times \frac{1}{(q - p')^2 - m_{P_{k_3}}^2 + i\epsilon}, \tag{B10}$$

with $m_{V_{k_1}}$, $m_{V_{k_2}} = m_{K^*}$ being the masses of the two vector mesons which couple to K_S^* in the triangular loop of Fig. 8 and $m_{P_{k_3}}$ is the mass of the exchanged pseudoscalar. Using Lorentz covariance, the integral of Eq. (B10) can be written as

$$I_\nu^{(k_1k_2k_3)} = a^{(k_1k_2k_3)}k_\nu + b^{(k_1k_2k_3)}p_\nu + c^{(k_1k_2k_3)}k'_\nu + d^{(k_1k_2k_3)}p'_\nu, \tag{B11}$$

and we need to determine the coefficients $a^{(k_1k_2k_3)}$, $b^{(k_1k_2k_3)}, \cdots$ appearing in this expression. The momentum and mass assignations for the particles involved in the triangular loop diagrams is shown in Fig. 13.

The determination of the four coefficients of Eq. (B11) can be done by making use of the Feynman parametrization and writing

$$\frac{1}{\alpha\beta\gamma} = 2\int_0^1 dx \int_0^x dy \frac{1}{[\alpha + (\beta - \alpha)x + (\gamma - \beta)y]^3}, \tag{B12}$$

where

$$\alpha \equiv q^2 - m_{V_{k_1}}^2, \qquad \beta \equiv (p + k - q)^2 - m_{K^*}^2, \qquad \gamma = (q - p')^2 - m_{P_{k_3}}^2. \tag{B13}$$

In this way,

$$[\alpha + (\beta - \alpha)x + (\gamma - \beta)y] = q'^2 + r^{(k_1k_2k_3)}, \tag{B14}$$

where we have defined

$$q' \equiv q - (p + k)(x - y) + p'y, \tag{B15}$$

and

$$r^{(k_1k_2k_3)} = -(x - y)[(m_V^2 + m_{K^*}^2 + 2p \cdot k)(x - y - 1) + 2p' \cdot (p + k)y + m_{V_{k_2}}^2] + [(1 - y)m_\pi^2 - m_{P_{k_3}}^2]y + m_{V_{k_1}}^2(x - 1) \tag{B16}$$

Using Eqs. (B12), (B14), (B15), (B16), and the relation

$$\int \frac{d^4q'}{(2\pi)^4}\frac{1}{(q'^2 + r + i\epsilon)^3} = \frac{i}{2^5\pi^2(r + i\epsilon)}, \tag{B17}$$

we can identify the coefficients in Eq. (B11),

$$a^{(k_1k_2k_3)} = b^{(k_1k_2k_3)} = \frac{1}{2^4\pi^2}\int_0^1 dx \int_0^x dy \frac{(x - y)}{r^{(k_1k_2k_3)} + i\epsilon},$$
$$c^{(k_1k_2k_3)} = \frac{1}{2^4\pi^2}\int_0^1 dx \int_0^x dy \frac{1}{r^{(k_1k_2k_3)} + i\epsilon},$$
$$d^{(k_1k_2k_3)} = \frac{1}{2^4\pi^2}\int_0^1 dx \int_0^x dy \frac{(y - 1)}{r^{(k_1k_2k_3)} + i\epsilon}. \tag{B18}$$

[1] J. Adams *et al.* (STAR Collaboration), Phys. Rev. C **71**, 064902 (2005).
[2] M. M. Aggarwal *et al.* (STAR Collaboration), Phys. Rev. C **84**, 034909 (2011).
[3] K. Aamodt *et al.* (ALICE Collaboration), Phys. Rev. Lett. **105**, 252301 (2010).
[4] B. B. Abelev *et al.* (ALICE Collaboration), Phys. Rev. C **91**, 024609 (2015).
[5] T. Blum, L. Karkkainen, D. Toussaint, and S. Gottlieb, Phys. Rev. D **51**, 5153 (1995).
[6] C. Song and V. Koch, Phys. Rev. C **55**, 3026 (1997).
[7] R. Rapp and E. V. Shuryak, Phys. Rev. Lett. **86**, 2980 (2001).
[8] P. Braun-Munzinger, D. Magestro, K. Redlich, and J. Stachel, Phys. Lett. B **518**, 41 (2001).
[9] S. Cho and S. H. Lee, arXiv:1509.04092.

[10] L. Roca, E. Oset, and J. Singh, Phys. Rev. D **72**, 014002 (2005).
[11] L. S. Geng, E. Oset, L. Roca, and J. A. Oller, Phys. Rev. D **75**, 014017 (2007).
[12] C. Daum *et al.* (ACCMOR Collaboration), Nucl. Phys. **B187**, 1 (1981).
[13] C. Patrignani *et al.* (Particle Data Group), Chin. Phys. C **40**, 100001 (2016) and 2017 update.
[14] L. Roca, A. Hosaka, and E. Oset, Phys. Lett. B **658**, 17 (2007).
[15] F. Aceti, J. J. Xie, and E. Oset, Phys. Lett. B **750**, 609 (2015).
[16] F. Aceti, J. M. Dias, and E. Oset, Eur. Phys. J. A **51**, 48 (2015).
[17] J. Wess and B. Zumino, Phys. Lett. B **37**, 95 (1971).
[18] E. Witten, Nucl. Phys. **B223**, 422 (1983).
[19] Y. S. Oh, T. Song, and S. H. Lee, Phys. Rev. C **63**, 034901 (2001).
[20] A. Martinez Torres, K. P. Khemchandani, F. S. Navarra, M. Nielsen, and L. M. Abreu, Phys. Rev. D **90**, 114023 (2014); **93**, 059902(E) (2016).
[21] L. M. Abreu, K. P. Khemchandani, A. Martinez Torres, F. S. Navarra, and M. Nielsen, Phys. Lett. B **761**, 303 (2016).
[22] S. Cho and S. H. Lee, Phys. Rev. C **88**, 054901 (2013).
[23] M. Bando, T. Kugo, S. Uehara, K. Yamawaki, and T. Yanagida, Phys. Rev. Lett. **54**, 1215 (1985).
[24] M. Bando, T. Kugo, and K. Yamawaki, Phys. Rep. **164**, 217 (1988).
[25] U. G. Meissner, Phys. Rep. **161**, 213 (1988).
[26] M. Harada and K. Yamawaki, Phys. Rep. **381**, 1 (2003).
[27] D. Gamermann, E. Oset, and B. S. Zou, Eur. Phys. J. A **41**, 85 (2009).
[28] H. Nagahiro, L. Roca, and E. Oset, Eur. Phys. J. A **36**, 73 (2008).
[29] K. P. Khemchandani, H. Kaneko, H. Nagahiro, and A. Hosaka, Phys. Rev. D **83**, 114041 (2011).
[30] K. P. Khemchandani, A. Martinez Torres, H. Kaneko, H. Nagahiro, and A. Hosaka, Phys. Rev. D **84**, 094018 (2011).
[31] R. F. Peierls, Phys. Rev. Lett. **6**, 641 (1961).
[32] W. S. Chung, G. Q. Li, and C. M. Ko, Phys. Lett. B **401**, 1 (1997).
[33] L. S. Geng and E. Oset, Phys. Rev. D **79**, 074009 (2009).
[34] F. Aceti, R. Molina, and E. Oset, Phys. Rev. D **86**, 113007 (2012).
[35] L. Roca and E. Oset, Phys. Rev. C **95**, 065211 (2017).
[36] F. Aceti, L. R. Dai, and E. Oset, Phys. Rev. D **94**, 096015 (2016).
[37] A. Martinez Torres, L. S. Geng, L. R. Dai, B. X. Sun, E. Oset, and B. S. Zou, Phys. Lett. B **680**, 310 (2009).
[38] A. Ilner, D. Cabrera, C. Markert, and E. Bratkovskaya, Phys. Rev. C **95**, 014903 (2017).
[39] A. Ilner, J. Blair, D. Cabrera, C. Markert, and E. Bratkovskaya, arXiv:1707.00060.
[40] P. Koch, B. Muller, and J. Rafelski, Phys. Rep. **142**, 167 (1986).
[41] R. Molina, D. Nicmorus, and E. Oset, Phys. Rev. D **78**, 114018 (2008).